



**HAL**  
open science

# A graph-based approach to glacier flowline extraction: An application to glaciers in Switzerland

Nicolas Le Moine, Pierre-Stéphane Gsell

► **To cite this version:**

Nicolas Le Moine, Pierre-Stéphane Gsell. A graph-based approach to glacier flowline extraction: An application to glaciers in Switzerland. *Computers & Geosciences*, 2015, 85 (Part A), pp.91-101. 10.1016/j.cageo.2015.09.010 . hal-01211407

**HAL Id: hal-01211407**

**<https://hal.sorbonne-universite.fr/hal-01211407>**

Submitted on 5 Oct 2015

**HAL** is a multi-disciplinary open access archive for the deposit and dissemination of scientific research documents, whether they are published or not. The documents may come from teaching and research institutions in France or abroad, or from public or private research centers.

L'archive ouverte pluridisciplinaire **HAL**, est destinée au dépôt et à la diffusion de documents scientifiques de niveau recherche, publiés ou non, émanant des établissements d'enseignement et de recherche français ou étrangers, des laboratoires publics ou privés.

# A graph-based approach to glacier flowline extraction: an application to glaciers in Switzerland

Nicolas Le Moine<sup>a,\*</sup>, Pierre-Stéphane Gsell<sup>a</sup>

<sup>a</sup>*Sorbonne Universités, UPMC Univ. Paris 06, CNRS, EPHE, UMR Metis*

---

## Abstract

In this paper we propose a new, graph-based approach to glacier segmentation and flowline extraction. The method, which requires a set of glacier contours and a Digital Elevation Model (DEM), consists in finding an optimum branching that connects a set of vertices belonging to the topological skeleton of each glacier. First, the challenges associated with glacier flowline extraction are presented. Then, the three main steps of the method are described: the skeleton extraction and pruning algorithm, the definition and computation of a travel cost between all pairs of skeleton vertices, and the identification of the directed minimum spanning tree in the resulting directed graph. The method, which is mainly designed for valley glaciers, is applied to glaciers in Switzerland.

*Keywords:* glacier flowline, skeleton, discrete curve evolution, optimum branching, directed minimum spanning tree

---

## 1. Introduction

### 1.1. Glacier morphology

Glaciers are moving ice bodies which flow under their own weight, due to the accumulation of solid precipitations on the higher slopes of a mountain range. As the strain rate increases, ice viscosity decreases and the accumulated ice literally ‘flows’ downslope. Bahr and Peckham (1996) first explicitly drew a parallel between rivers and valley glaciers (i.e. glaciers that are confined by topography, as opposed to ice caps). They showed that glaciers also

---

\*Corresponding author

*Email address:* nicolas.le\_moine@upmc.fr (Nicolas Le Moine)

9 exhibit branching topologies, and computed classical river network indices  
10 such as bifurcation and area ratios for glacier networks. This analogy stems  
11 from the fact that in most recent orogens where valley glaciers are found (the  
12 Alps, the Andes, the Himalayas, the Rocky Mountains, etc.), glacier incep-  
13 tion took place in a topography previously shaped by fluvial erosion (Gsell et  
14 al., 2014). Bahr and Peckham also pointed out that self-similarity properties  
15 could provide a ‘lever arm’ for tackling glacier flow dynamics for complex  
16 geometries, just as these properties are used for treating subgrid, hydraulic  
17 propagation in complex river networks with concepts such as the Geomorpho-  
18 logical Instantaneous Unit Hydrograph (Rodríguez-Iturbe and Valdés, 1979;  
19 Gupta et al., 1980). One of the reasons why this approach has not been given  
20 much attention is maybe the difficulty lying in the first step of identifying  
21 networks of glacier flowlines.

### 22 *1.2. Limits of classical drainage network extraction methods*

23 Figure 1 shows the downstream region of the Rhone glacier in Switzer-  
24 land. In fluvial morphology, we typically find cross-sections such as A–A’  
25 with a concave topography in the talweg. This translates into V- or U-  
26 shaped (for former glacial valleys) elevation contours, with the lowest point  
27 roughly in the medial axis of the talweg. Hence, river network extraction  
28 from a DEM is relatively straightforward, except for problems such as flat  
29 areas or closed depressions (see e.g. Garbrecht and Martz, 1997; Martz and  
30 Garbrecht, 1998).

31  
32 Things are more complicated for ice-covered areas. In the accumulation  
33 (higher) area of the glacier, where hillslopes as well as valley floors are ice-  
34 covered, the topography is still concave (B–B’): the surface of the ice is more  
35 or less homothetic to the bedrock surface (with lower roughness though). In  
36 contrary, in the ablation area the glacier is limited to a narrow ice tongue  
37 confined between lateral, ice-free hillslopes. Since ice thickness is maximum  
38 in the medial axis of the ice tongue, we have a convex cross-section (C–C’)  
39 with seemingly two talwegs on each side of the glacier. Elevation contours  
40 in this area have the shape of a W with its two wedges pointing upstream,  
41 as opposed to the single wedge in concave topography. The central flowline  
42 of the glacier (i.e. the line of maximum ice thickness), which is also typically  
43 the line of the bedrock talweg, is a local maximum and not a local minimum  
44 of the ice surface (it looks like is a local water divide). Therefore, it cannot  
45 be extracted in a stable way from a DEM with classical algorithms.

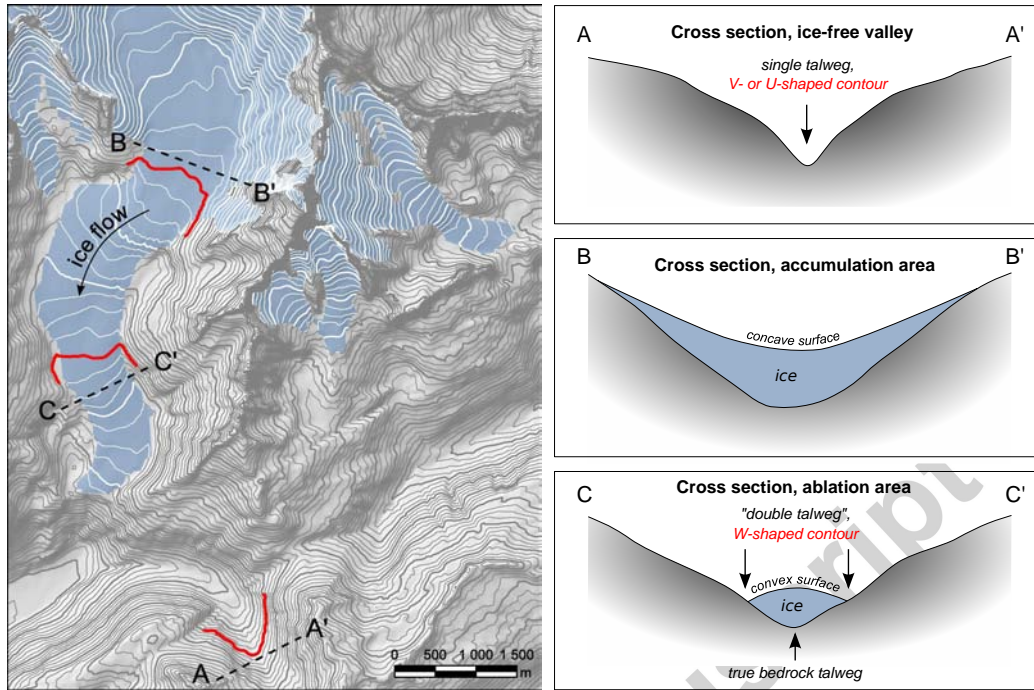


Figure 1: Illustration of the spurious ‘double talweg’ in glacial landscape. This feature mainly appears in the glacier’s ablation area where a narrow ice tongue is confined in a valley (C–C’). On a map, elevation contours in this area have the shape of a W with its two wedges pointing upstream, whereas contours in classical (ice-free) valleys are V- or U-shaped with a single wedge pointing upstream (A–A’).

### 46 1.3. Automatic methods for glacier flowline extraction

47 The problem of glacier flowline extraction has received some attention  
 48 recently, due to the need of feeding glacier databases with attributes such  
 49 as glacier length. A flowline or a set of flowlines has to essentially meet  
 50 two requirements: (i) to stay as far as possible from the glacier boundary,  
 51 and (ii) to cross elevation contours orthogonally. Le Bris and Paul (2013)  
 52 propose to construct a set of waypoints located at the center of ‘traverses’  
 53 drawn perpendicular to a single, rectilinear ‘main axis’, and then connect  
 54 them. However, the method can only extract one centerline per glacier.  
 55 Kienholz et al. (2014) use a more complex approach based on a cost function  
 56 which quantifies the trade-off between the two requirements; a set of flowlines  
 57 is then extracted between glacier heads and a single snout (terminus) per  
 58 glacier. Other methods apply alternate procedures in the accumulation and

59 ablation zones (Machguth and Huss, 2014), also resulting in a large number  
60 of parameters.

#### 61 *1.4. Objectives of the study*

62 In this paper, a new method is presented that aims at extracting glacier  
63 flowlines with an emphasis on preserving their tree-like structure, i.e. the  
64 structure of tributaries within the glacier.

65  
66 As in Le Bris and Paul (2013), our method first identifies a set of way-  
67 points (i.e., vertices of a graph) that are subsequently connected. However  
68 these waypoints are identified with a more general operation called skele-  
69 tonization. Once these waypoints are identified (including special ‘snout’  
70 vertices), we compute a travel cost between every pair of them: the cost  
71 function is designed so as to penalize displacements that deviate from the  
72 steepest slope direction. The main difference with Kienholz et al. (2014) is  
73 the formulation of an anisotropic cost function. The final step is to construct  
74 a directed minimum spanning tree (DMST) that allows to visit all waypoints  
75 at minimal cost, starting from a snout (root) vertex. Edges of this DMST  
76 meet the two requirements: they stay ‘far’ from the glacier’s boundary (since  
77 they link waypoints belonging to the skeleton), and they deviate little from  
78 the steepest slope direction since they are least-cost paths with respect to  
79 the slope-dependent cost function. The overall procedure requires only 5 pa-  
80 rameters, in contrast with other methods (e.g. 16 parameters in Kienholz et  
81 al., 2014 and 17 in Machguth and Huss, 2014).

82  
83 The method is mainly designed for valley glaciers, as ice caps usually do  
84 not exhibit strong branching topologies. It is tested on a dataset of Swiss  
85 glaciers (Figure 2a), covering a total area of 1200 km<sup>2</sup> and mainly located  
86 in the headwaters of the Rhone, Rhine, and Danube rivers. The steps of the  
87 method are illustrated with a focus on a particular glacier complex in the  
88 Bernese Alps (Figure 2b), straddling the water divide between the Rhone  
89 and Rhine rivers.

## 90 **2. Data**

### 91 *2.1. Digital Elevation Model*

92 In this study we use the 25-meter Digital Elevation Model from the Swiss  
93 Federal Office of Topography (SwissTopo, 2004).

94 *2.2. Randolph Glacier Inventory (RGI) glacier contours*

95 Glacier outlines are taken from the Randolph Glacier Inventory (RGI,  
96 Arendt et al., 2012). The RGI provides a segmentation of glacier complexes  
97 (continuous ice bodies) into individual glaciers; we chose to dissolve (re-  
98 aggregate) these elements and to work with the complexes in order test the  
99 ability of our approach to identify multiple snouts in such complexes. The  
100 segmentation is not a prerequisite and is even a by-product of our method.

101 **3. Skeleton extraction and pruning**

102 *3.1. Glacier flowlines as a topological skeleton*

103 The method proposed by Le Bris et al. (2013), which consists in picking  
104 the midpoints of ‘traverses’ drawn orthogonally to the glacier’s ‘main axis’, is  
105 actually related to a topological operation called skeletonization, or medial-  
106 axis transform. A first, intuitive definition is the analogy with a grassfire  
107 (Blum, 1967): if one ‘sets fire’ simultaneously at all points on the border  
108 of a grass field enclosed in the object’s boundary, then the skeleton is the  
109 set of points where two or more firefronts meet (see Figure 3a). The result  
110 (Figure 3b) is a ‘thinned’ version of the object (i.e., a set of edges, namely  
111 a graph) that preserves its essential geometrical and topological features (in  
112 the example of Figure 3, the skeleton edges look like the veins of the leaf).  
113 We will see that this is a first interesting step to glacier flowline extraction.

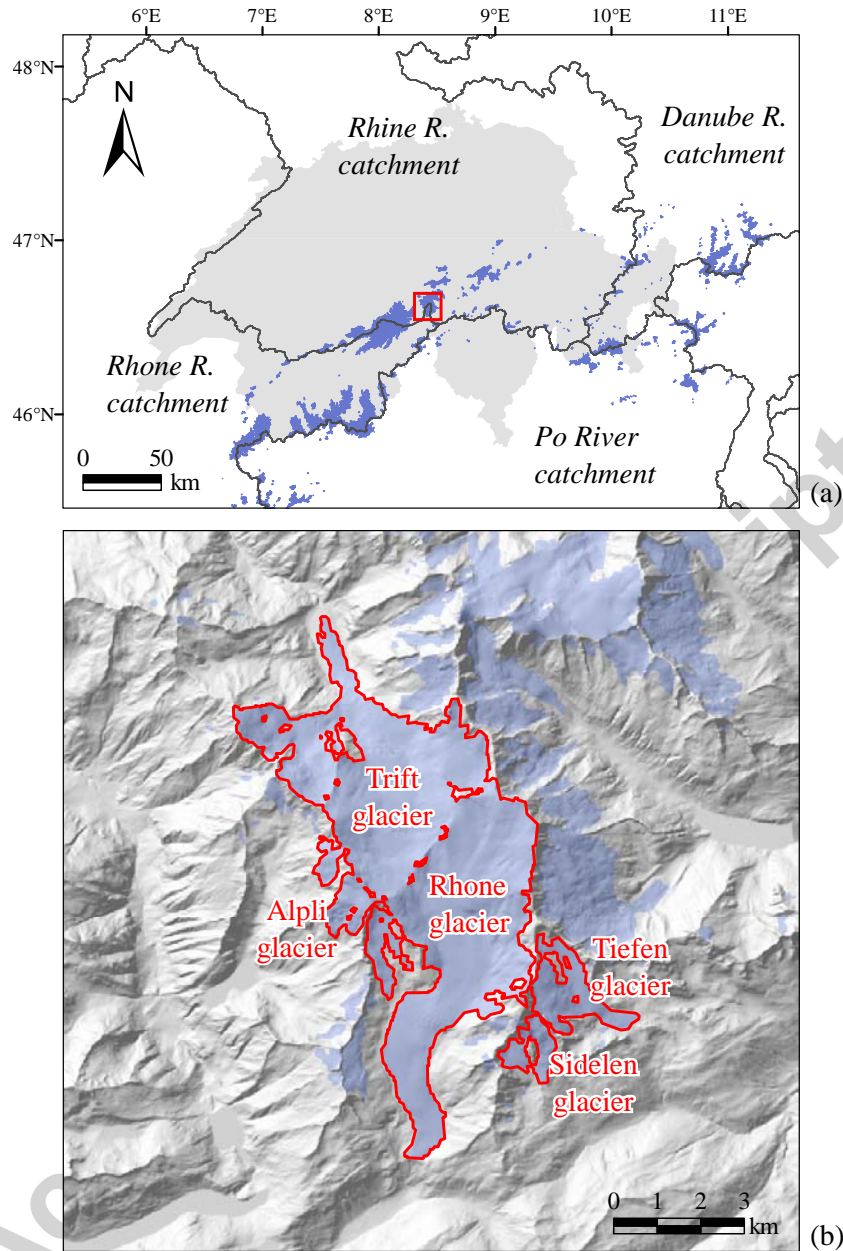


Figure 2: Area covered by this study. (a) Map of Switzerland with glacier contours in dark blue. (b) Zoom on the Rhone-Trift glacier complex illustrating the steps throughout the paper. This complex covers  $35.8 \text{ km}^2$  and includes two large glaciers: the Rhone glacier ( $15.9 \text{ km}^2$ ) and the Trift glacier ( $16.6 \text{ km}^2$ ) as well as a number of smaller ones (e.g. Tiefen, Sidelen and Alpli glaciers).

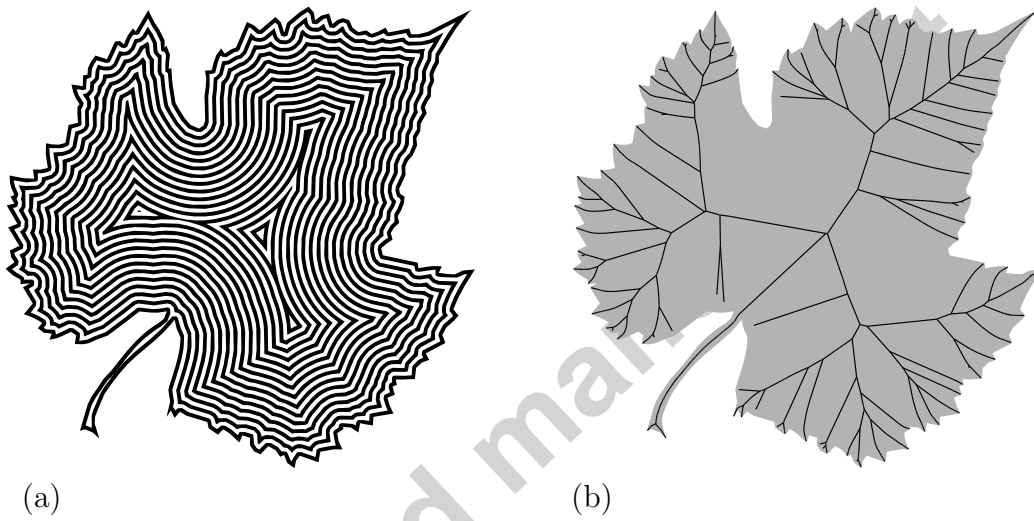


Figure 3: Grassfire analogy of the skeletonization: (a) propagation of the 'firefronts'; (b) resulting skeleton i.e. the set of points where two or more fronts meet.



114 3.2. Skeletonization using Voronoi tessellation

115 A second definition of the skeleton uses the concept of maximal disk (or  
 116 maximal ball in dimensions higher than 2). A disk  $\mathcal{B}$  is said to be maximal  
 117 in set  $\mathcal{D}$  if it is completely included in  $\mathcal{D}$ , and such that if it is contained in  
 118 any other disc  $\mathcal{B}'$  then  $\mathcal{B}'$  is not completely included in  $\mathcal{D}$ . Mathematically,

$$\mathcal{B} \text{ is a maximal disk in set } \mathcal{D} \text{ iif } \begin{cases} \mathcal{B} \subseteq \mathcal{D} \\ \mathcal{B} \subset \mathcal{B}' \Rightarrow \mathcal{B}' \not\subseteq \mathcal{D} \end{cases} \quad (1)$$

119 A maximal disk  $\mathcal{B}(\mathbf{s})$  centered at point  $\mathbf{s}$  is entirely contained in  $\mathcal{D}$  and is  
 120 interiorly tangent to the boundary  $\partial\mathcal{D}$  in at least two different points, called  
 121 generating points: these are two locations where firefronts originate from in  
 122 the grassfire analogy, and they meet at the center of a maximal disk. The  
 123 skeleton  $S(\mathcal{D})$  can be defined as the set of the centers of all maximal disks  
 124 in  $\mathcal{D}$ :

$$S(\mathcal{D}) = \{ \mathbf{s} \mid \mathcal{B}(\mathbf{s}) \text{ is a maximal disk in } \mathcal{D} \} \quad (2)$$

125 Figure 4 illustrates this definition.  $Gen(\mathbf{s}) \subset \partial\mathcal{D}$  denotes the generating  
 126 points of the skeletal point  $\mathbf{s} \in S(\mathcal{D})$ .

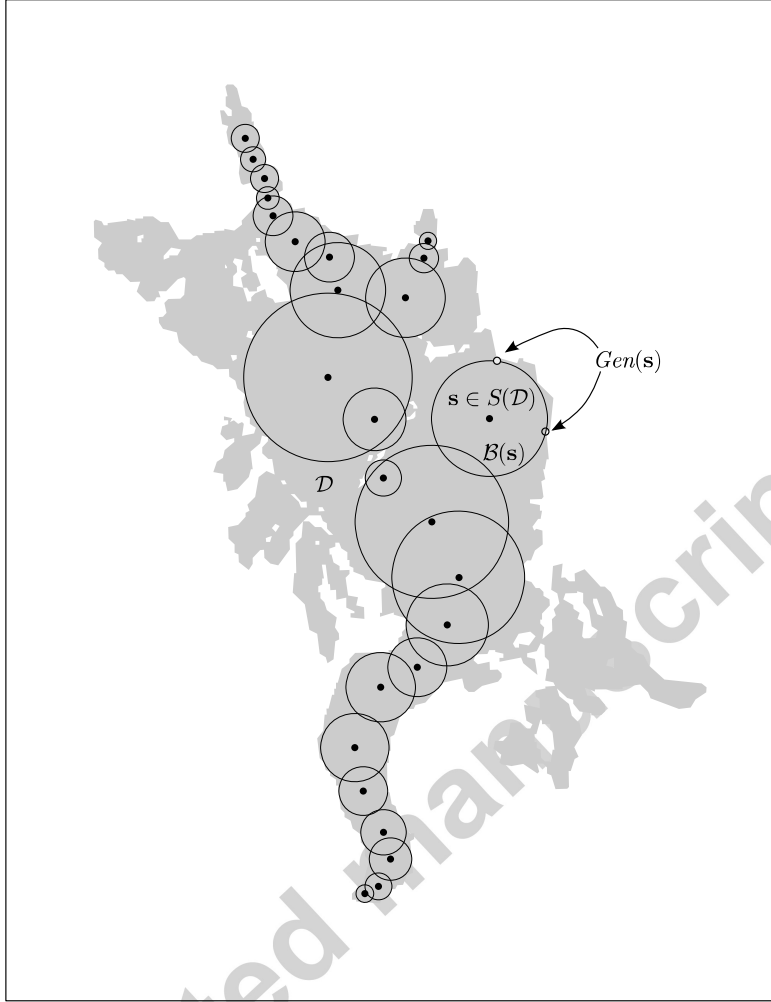


Figure 4: Definition of skeleton  $S(\mathcal{D})$  as the set of centers of all maximal disks in  $\mathcal{D}$  (gray shape).  $Gen(s)$  denotes the generating points of the skeletal point  $s$ .

127 One possibility to generate the skeleton is to implement a ‘grassfire’ al-  
 128 gorithm. Given the previous definition, another method uses the Voronoi  
 129 tessellation (see e.g. Brandt and Algazi, 1992) of a set of points (input sites)  
 130 sampled along the boundary (see Figure 5). Each Voronoi region represents  
 131 the area closest to a boundary input site, and is delimited by several edges:  
 132 hence, each edge  $\mathcal{E}$  is a segment of the perpendicular bisector of a *pair* of  
 133 input sites. To show the similarity with the previous results, we call this pair  
 134 the generating pair  $Gen(\mathcal{E})$  of the edge. As the number  $n$  of input sites sam-

135 pled on the boundary increases ( $n \rightarrow \infty$ ), the set of edges of the tessellation  
 136 that are contained in the domain  $\mathcal{D}$  converges to the exact skeleton.

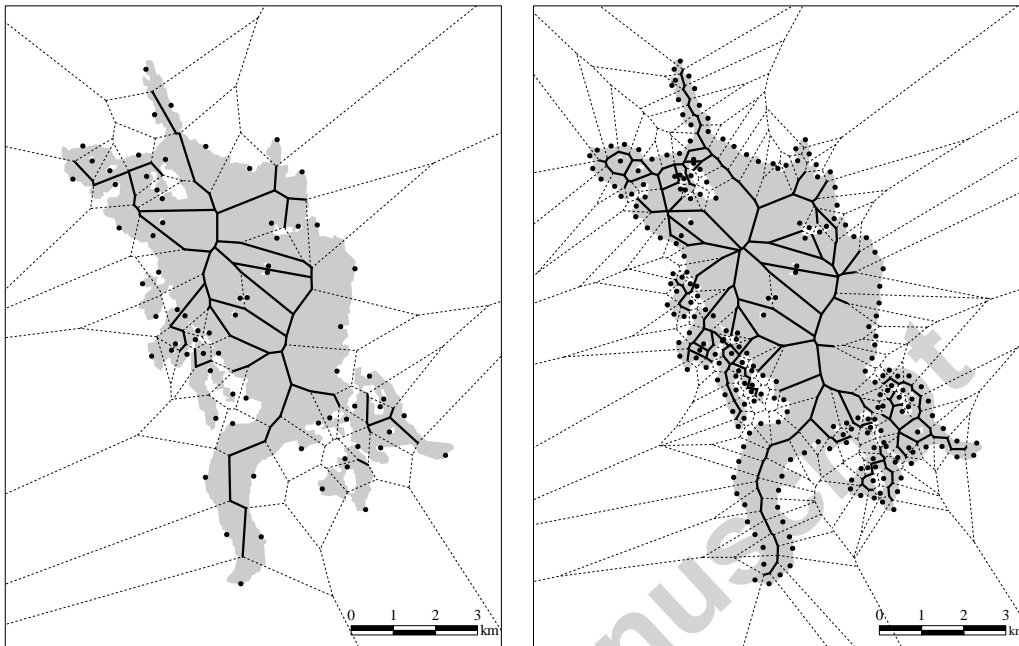


Figure 5: Skeletonization using the Voronoi tessellation of a set of boundary input sites. The set of internal edges of the tessellation (solid black lines) converges to the skeleton as the number of points on the boundary increases (left: one point every 2000 m ; right: one point every 500 m).

137 We used the Qhull library (Barber et al., 1996) to generate the tesse-  
 138 lation. It allows to retrieve not only the Voronoi edges but also the pair  
 139 of generating input sites (boundary points) for each edge, a highly valuable  
 140 information for the subsequent steps. It is worth noting that the object may  
 141 have inner boundaries (‘holes’ in the shape, such as inner rocks for a glacier),  
 142 which will translate into cycles in the skeletal graph.

143

144 RGI glacier contours were first densified so as to have at least one point  
 145 every 50 m along the boundary, before running the tessellation with Qvoronoi.  
 146 All subsequent steps were then performed under Scilab (Scilab Entreprises,  
 147 2012), using the CLaRiNet library (Le Moine, 2013).

148 *3.3. Skeleton pruning through Discrete Curve Evolution*

149 As mentioned previously, the set of edges obtained with the Voronoi tessellation is only an approximation of the skeleton. Moreover, due to the noise in the boundaries, insignificant boundary features can generate skeleton edges which do not reflect essential topological properties. Hence, we need to simplify, or ‘prune’, the skeleton i.e. remove many spurious edges.

154

155 In this study we use the pruning algorithm of Bai et al. (2007), who point out that not all  $n$  boundary points significantly contribute to the shape of the object: only a relatively small subset of these boundary (input) sites may be sufficient to describe the overall shape. Hence, if we select  $k \leq n$  points on the boundary, we define a partition of the contour into  $k$  contour segments (subarcs). The pruning rule is to remove all skeleton edges whose generating points lie on a same contour segment, as illustrated in Figure 6. It is important to note that this pruning process is not equivalent to reducing the number of input sites in the Voronoi tessellation (i.e. moving from right to left in Figure 5): the pruning removes some edges but the geometry of the remaining ones is not altered.

165

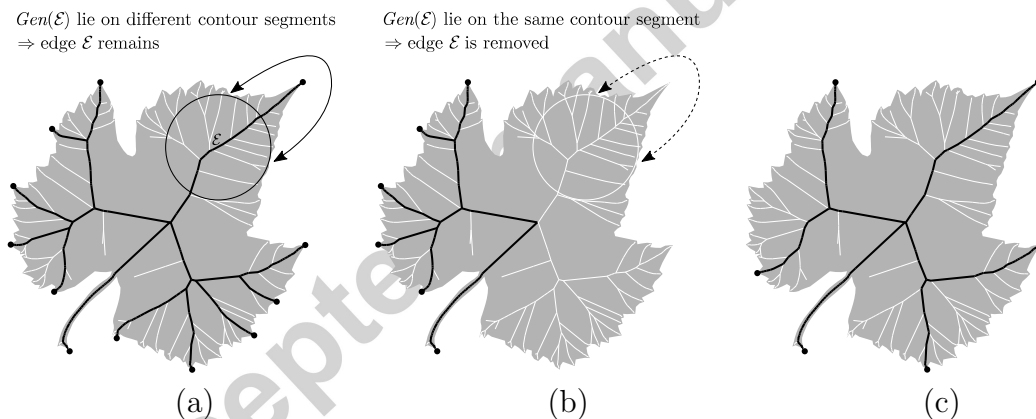


Figure 6: Pruning of the skeleton based on contour partitioning. Skeleton edges which have their generating points lying on a same contour segment are removed (in white). (a) Partition with  $k = 12$  points; (b)  $k = 6$  points; (c)  $k = 6$  points but at different locations.

166 The problem is to select the  $k$  most relevant points; Bai et al. (2007) propose to reduce the number of boundary points from  $n$  to  $k < n$  through Discrete Curve Evolution (DCE).

169

170 Let  $\mathbf{c}_1, \dots, \mathbf{c}_n$  be the  $n$  input sites sampled on the boundary, and let  
 171  $\mathbf{u}_{i-1,i} = \mathbf{c}_i - \mathbf{c}_{i-1}$  and  $\mathbf{u}_{i,i+1} = \mathbf{c}_{i+1} - \mathbf{c}_i$  be the vectors of the boundary edges  
 172 incident to point  $\mathbf{c}_i$  (Figure 7). The contribution of this site to the overall  
 173 shape is (Latecki and Lakämper, 2002):

$$K(\mathbf{c}_i) = \frac{\theta_i \|\mathbf{u}_{i-1,i}\| \|\mathbf{u}_{i,i+1}\|}{\|\mathbf{u}_{i-1,i}\| + \|\mathbf{u}_{i,i+1}\|} \quad (3)$$

where

$$\theta_i = \widehat{(\mathbf{u}_{i-1,i}, \mathbf{u}_{i,i+1})} = \arccos\left(\frac{\mathbf{u}_{i-1,i} \cdot \mathbf{u}_{i,i+1}}{\|\mathbf{u}_{i-1,i}\| \|\mathbf{u}_{i,i+1}\|}\right) \operatorname{sgn}(\det(\mathbf{u}_{i-1,i}, \mathbf{u}_{i,i+1}))$$

174 is the oriented turn angle at point  $\mathbf{c}_i$  (trigonometric, i.e. measured counter-  
 175 clockwise). This contribution is usually defined in 2D (planar computation),  
 176 but there is no difficulty in extending it to a 3D curve. However, even if  
 177 glaciers are located on steep topography, they remain objects in the geo-  
 178 graphical space i.e. with a rather flat aspect ratio, so that the addition of  
 179 the vectors' z-coordinate would not change the contributions dramatically.

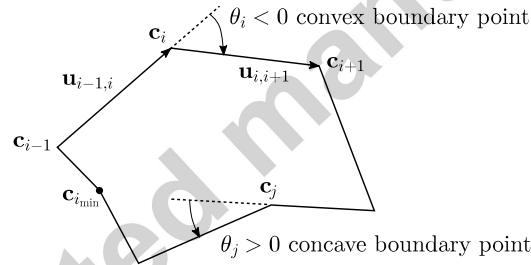


Figure 7: Definition of the turn angle at a boundary point.

180 Since contours are closed, we set  $\mathbf{c}_{n+1} = \mathbf{c}_1$  and  $\mathbf{c}_0 = \mathbf{c}_n$ . If boundary  
 181 points are sorted clockwise (i.e. with the ‘inside’ on the right and the ‘outside’  
 182 on the left when moving along the boundary, as in the ESRI<sup>®</sup> shapefile  
 183 format), then:

- 184 •  $K$  is negative for a convex point (clockwise turn), and positive for a  
 185 concave point (counterclockwise turn),
- 186 • the higher the absolute value  $|K|$ , the higher the contribution to the  
 187 overall shape (through great segment lengths and/or large turn angle).

188 A point lying on a straight contour portion, i.e. such that  $\theta = 0$ , will  
 189 have a zero contribution (i.e. it can be removed without any loss of  
 190 shape information).

191 We start the DCE with the  $n$  initial input sites and we removes the point  
 192  $\mathbf{c}_{i_{\min}}$  having the lowest absolute value  $|K(\mathbf{c}_{i_{\min}})|$ , thus leading to a simplified  
 193 contour called DCE level  $n-1$ . The metric  $K$  is again computed for the  $n-1$   
 194 remaining points, and the procedure is repeated  $p$  times to obtain a hierar-  
 195 chical set of contour partitions, called DCE level  $n-2, n-3, \dots, k = n-p$ .  
 196 At each iteration, we remove the skeleton edges whose generating points lie  
 197 on a same contour segment of DCE level  $k = n-p$ , and these edges are  
 198 assigned the level  $k$ . Since we need at least two points on the contour to  
 199 define a partition, the highest possible level is  $k = 2$ . Figure 6c actually rep-  
 200 resents DCE level 6 of the leaf, and in Figure 8 we show the final hierarchy  
 201 of skeleton edges.

202  
 203 If the shape has one or several inner boundaries, we simply add a loop on  
 204 the boundaries in order to find the least-contributing site at each iteration.



Figure 8: Hierarchy of skeleton edges obtained at the end of the pruning algorithm: we can stop at any level in this hierarchy.

#### 205 4. Identification of snout vertices

206 In the previous section we illustrated the skeleton extraction and pruning  
 207 with a simple shape (a leaf); we now apply these methods to RGI contours

208 of Swiss glaciers. The main issues will be to decide the level  $k$  at which we  
 209 should extract the skeleton for each glacier, and to use elevation data in order  
 210 to identify snout and head vertices.

#### 211 4.1. Choice of DCE level for each glacier

212 Consider a glacier with area  $A$ . Clearly, the larger the glacier, the more  
 213 points will be needed on its boundary to correctly describe its shape or skele-  
 214 ton, i.e. the higher we will need to stay in the DCE hierarchy. Conversely,  
 215 a small glacier with a single main axis without tributary could be correctly  
 216 described at DCE level  $k = 2$ . A selection rule of thumb  $k = f(A)$  was  
 217 devised empirically upon visual appreciation:

$$(k - 2) = \lfloor k_0 A^\gamma \rfloor$$

218 where  $\lfloor \cdot \rfloor$  is the floor function. We used  $k_0 = 13.5$  and  $\gamma = 0.8$  with  $A$  in  
 219  $\text{km}^2$ . For example, the skeleton of Rhone-Trift glacier complex, with an area  
 220  $A = 35.8 \text{ km}^2$ , is still correctly described at DCE level  $k = 2 + 13.5(35.8)^{0.8} =$   
 221  $238$ , i.e. with 238 sites on its boundary (Figure 9, left panel).

#### 222 4.2. Hierarchical snout identification

223 The next step is the orientation of the skeletal edges in order to identify  
 224 glacier snouts and heads. Indeed, skeletonization is a planar operation and  
 225 we do not know if a ‘leaf’ vertex in the skeleton corresponds to the beginning  
 226 of a flowline (‘head’ vertex), or to its end (‘snout’ vertex). Again, we will use  
 227 the results of the DCE algorithm to create a hierarchy of potential snouts.  
 228 A skeletal vertex  $\mathbf{s}$  is said to be a level- $k$  snout if it meets the three following  
 229 requirements:

- 230 (i)  $\mathbf{s}$  is a leaf vertex of the skeletal graph of DCE level  $k$ , i.e. having a  
 231 degree (number of incident edges)  $d = 1$ ,
- 232 (ii)  $\mathbf{s}$  is at an elevation lower than its closest vertex  $\mathbf{s}'$  of degree  $d \neq 2$  in the  
 233 level  $k$  skeleton graph.  $\mathbf{s}'$  is such that all vertices on the path between  
 234  $\mathbf{s}$  and  $\mathbf{s}'$  have degree 2: in the following we will call such a sequence of  
 235 vertices of degree 2 (except the two extremal vertices) a *stretch*.
- 236 (iii) the generating points  $Gen(\mathcal{E}_{\mathbf{s}})$  of its unique incident edge  $\mathcal{E}_{\mathbf{s}}$  (pendant  
 237 edge) lie on either side of an input site which is a local topographic  
 238 minimum in the DCE level  $k$ .

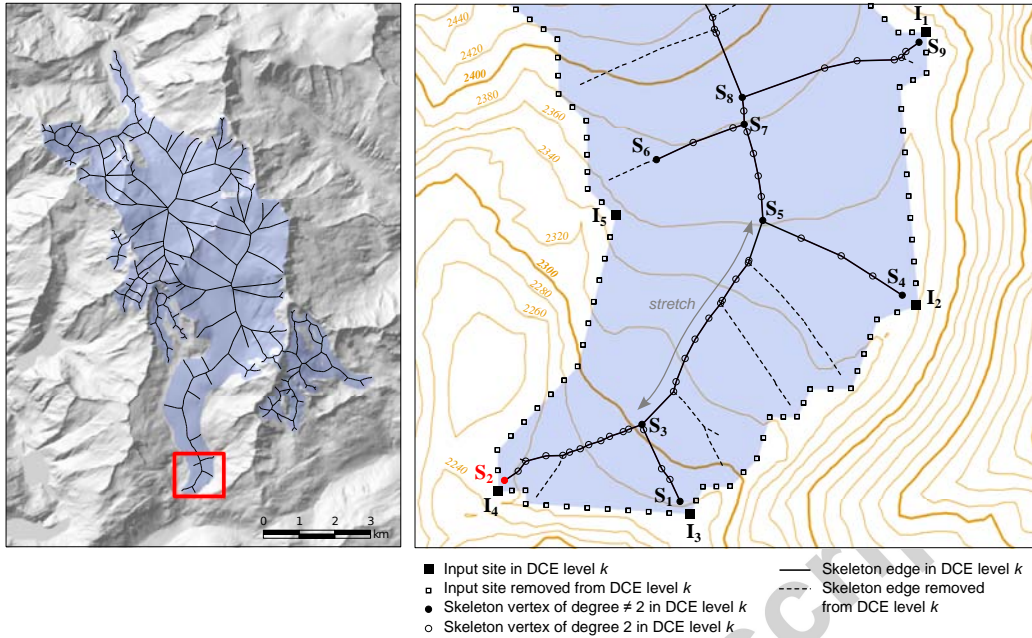


Figure 9: Definition of a snout vertex in the skeleton pruned at DCE level  $k$  ( $k = 238$  here).

239 These seemingly complicated requirements translate the more intuitive  
 240 notion that an edge is at a snout if it points downslope in a locally convex  
 241 portion of the boundary that also points downslope, as shown in Figure 9.



242 On Figure 9, skeleton edges at level  $k$  are drawn in solid black lines, while  
 243 edges that have been pruned at earlier levels are drawn with dotted lines.  
 244 There are several ‘candidate’ snouts in this area: skeleton vertices  $\mathbf{S}_1$ ,  $\mathbf{S}_2$ ,  
 245  $\mathbf{S}_4$ ,  $\mathbf{S}_6$  and  $\mathbf{S}_9$ , which are all leaf vertices at the current pruning level, i.e.  
 246 meeting requirement (i). All these 5 vertices also satisfy requirement (ii),  
 247 since we have:

$$\begin{array}{ll}
 \text{Leaf vertex} & \text{Nearest vertex of degree } \neq 2 \\
 z(\mathbf{S}_1) & < z(\mathbf{S}_3) \\
 z(\mathbf{S}_2) & < z(\mathbf{S}_3) \\
 z(\mathbf{S}_4) & < z(\mathbf{S}_5) \\
 z(\mathbf{S}_6) & < z(\mathbf{S}_7) \\
 z(\mathbf{S}_9) & < z(\mathbf{S}_8)
 \end{array}$$

248 However, Table 1 shows that only one candidate satisfies the third re-  
 249 quirement:

Leaf vertex	Input site in DCE level $k$ that separates the vertex’s generating pair	Is requirement (iii) met ?
$\mathbf{S}_1$	$\mathbf{I}_3$	NO: $z(\mathbf{I}_2) > z(\mathbf{I}_3) > z(\mathbf{I}_4)$
$\mathbf{S}_2$	$\mathbf{I}_4$	YES: $z(\mathbf{I}_3) > z(\mathbf{I}_4) < z(\mathbf{I}_5)$
$\mathbf{S}_4$	$\mathbf{I}_2$	NO: $z(\mathbf{I}_1) > z(\mathbf{I}_2) > z(\mathbf{I}_3)$
$\mathbf{S}_6$	$\mathbf{I}_5$	NO
$\mathbf{S}_9$	$\mathbf{I}_1$	NO

Table 1: Check for requirement (iii) in the definition of snout vertices.

250 Hence, the only snout at level  $k$  in this part of the glacier is vertex  $\mathbf{S}_2$ . As  
 251 input sites are iteratively removed from the glacier’s outline in the DCE pro-  
 252 cess, the combination of requirements allows a robust identification of convex  
 253 portions of the boundary that point downslope, i.e. glacier tongues/snouts.  
 254 Finally, skeleton stretches which satisfy requirements (i) and (ii) but not re-  
 255 quirement (iii) are further removed.

256  
 257 Hence, we obtain a snout hierarchy tied to the edge hierarchy: with a  
 258 single threshold (the level  $k = f(A)$  of the DCE), we can extract both a set  
 259 of skeletal edges and a set of snouts for a given continuous ice body of area  $A$ .

260 4.3. Definition of skeleton waypoints

261 Let us have a closer look at the final pruned skeleton in Figure 10. The  
 262 solid black lines are the remaining edges while the black dots are just a subset  
 263 of the vertices in the pruned skeleton that we downsampled for simplicity  
 264 (these vertices are *waypoints* distant from at least 1000 m). Clearly the  
 265 skeleton edges are far from a set of flowlines, except maybe in the ablation  
 266 area. The location of glacier heads and snouts looks satisfying but major  
 267 flaws appear:

- 268 • many edges in the skeleton significantly deviate from the local steepest  
 269 slope direction, i.e. do not at all cross elevation contours at a right  
 270 angle,
- 271 • the skeleton has cycles (around inner rocks).

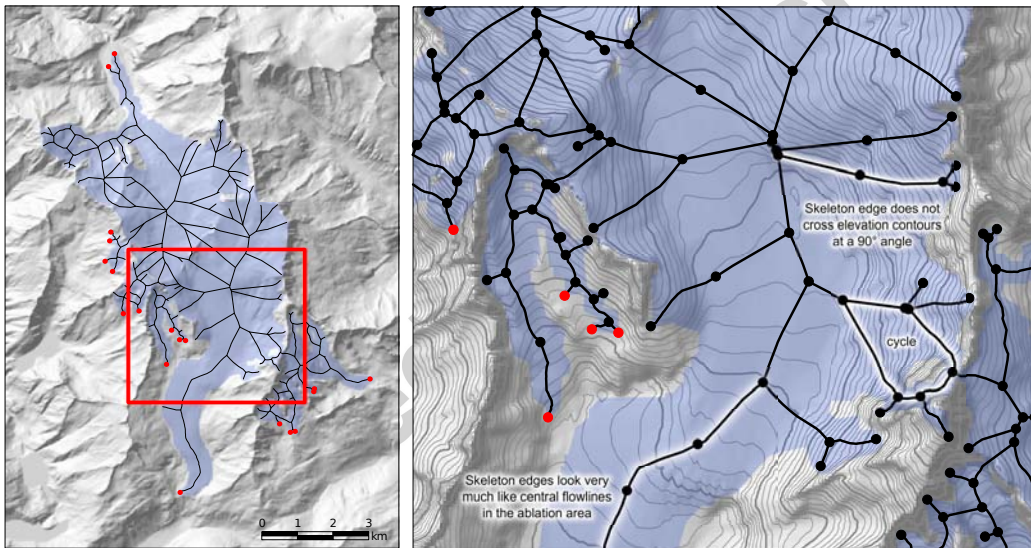


Figure 10: Example of flaws in the pruned skeletal graph, notably the deviation of skeleton edges from steepest slope directions and the presence of cycles. Black dots are a downsampled subset of skeleton vertices (waypoints), and red dots are snout vertices.

272 We will see that we can build another graph which links those same  
 273 skeleton vertices/waypoints, but which do not exhibit these flaws, provided  
 274 we can *quantify* what a ‘significant deviation from the local steepest slope  
 275 direction’ is.

276 **5. Construction of optimum branchings**

277 In this section we define a *cost function* that will allow us to rate how  
 278 much an edge between two vertices deviates from a slope line, and to select  
 279 a suitable set of edges.

280 *5.1. Rationale*

281 Douglas (1994) recalls that computing the least-cost path (with respect  
 282 to various factors such as slope, soil cover, etc.) between a point A and a  
 283 point B involves three steps:

- 284 1. the definition of a *cost of movement* for an elementary movement from  
 285 A to A' (close to A);
- 286 2. the computation of the *accumulated cost surface* spreading from the  
 287 starting point, that sums the costs of all elementary movements;
- 288 3. the construction of the least-cost path as the *slope line* of the accumu-  
 289 lated cost surface starting at B and ending at A (Warntz, 1957).

290 If we want a least-cost path to look like a steepest ascent or descent line,  
 291 we can figure out what the corresponding cost function has to look like by  
 292 reversing the three steps:

- 293 3. The least-cost path has to look like a topographical slope line (it will  
 294 never be a true one though, unless B is strictly upslope or downslope  
 295 from A)
- 296 2. This implies that the *accumulated cost surface* has to 'look like' the  
 297 topographical surface  $z$  around A;
- 298 1. It means that the local *cost of movement* has to 'look like' a *differential*  
 299 of the topographical surface, i.e. depend on its gradient  $\nabla z$ .

300 The next section presents a cost function designed according to this ra-  
 301 tionale.

302 *5.2. Definition of the cost function*

303 Consider an elementary displacement  $\delta \mathbf{x} = (dx, dy)$  from  $\mathbf{x} = (x, y)$  to  
 304  $\mathbf{x}' = (x', y') = \mathbf{x} + \delta \mathbf{x} = (x + dx, y + dy)$ . The cost of this elementary  
 305 displacement will be defined as:

$$\begin{aligned}
C_{\uparrow}(\mathbf{x}, \mathbf{x} + \delta\mathbf{x}) &= [z_{\max} - z(\mathbf{x})] - [z(\mathbf{x} + \delta\mathbf{x}) - z(\mathbf{x})] + \lambda\|\delta\mathbf{x}\| \\
&= \underbrace{\|\nabla z\|\|\delta\mathbf{x}\|}_{(1)} - \underbrace{(\nabla z) \cdot \delta\mathbf{x}}_{(2)} + \underbrace{\lambda\|\delta\mathbf{x}\|}_{(3)}
\end{aligned}$$

306 where  $\|\delta\mathbf{x}\| = \sqrt{dx^2 + dy^2}$  is the length of the displacement,  $\nabla z$  is the  
307 gradient vector of the topographic surface at point  $\mathbf{x}$ , and  $\lambda$  is a friction factor  
308 (scalar) in  $\text{m} \cdot \text{m}^{-1}$ . This cost is expressed in meters of potential energy and  
309 is the sum of three terms:

- 310 (1) is the maximum elevation (relative to  $z(\mathbf{x})$ ) we could reach with a  
311 displacement of length  $\|\delta\mathbf{x}\|$  starting at  $\mathbf{x}$ . By definition of the gradient,  
312 this maximum elevation is  $z_{\max} = \|\nabla z\|\|\delta\mathbf{x}\|$ , which is always positive.  
313 (2) is the elevation we actually reached with the displacement  $\delta\mathbf{x}$ , which  
314 is  $z' = (\nabla z) \cdot \delta\mathbf{x}$  (note that  $z'$  is algebraic and may be negative).  
315 Consequently, the difference (1) – (2), which is always positive whatever  
316 the displacement, is a measure of *how much higher* we could have gotten  
317 with a displacement of the same length. If the displacement is in the  
318 direction of the gradient (i.e. upslope) then  $\nabla z$  and  $\delta\mathbf{x}$  are colinear  
319 and  $(\nabla z) \cdot \delta\mathbf{x} = \|\nabla z\|\|\delta\mathbf{x}\|$ . Hence (1) and (2) cancel out in the  
320 case of a steepest *ascent*: the cost will be low. Conversely, if we move  
321 downslope,  $(\nabla z) \cdot \delta\mathbf{x}$  is negative and (1) – (2) is largely positive: the  
322 displacement is very costly.  
323 (3) is a friction term stabilizing the cost function: whatever the direction  
324 (upslope, downslope or along an elevation contour), there is always a  
325 cost  $\lambda$  for moving 1 meter across the surface. The effect is to smooth  
326 trajectories and to prevent paths from following too closely the small-  
327 scale irregularities on the surface.

328 We call  $C_{\uparrow}$  the *upslope* cost function, which is obviously not symmetric:

$$C_{\uparrow}(\mathbf{x}, \mathbf{x}') \neq C_{\uparrow}(\mathbf{x}', \mathbf{x})$$

329 The definition of  $C_{\uparrow}$  looks unusual, as classical cost functions (see e.g.  
330 Kienholz *et al.*, 2014) are simply the product of a scalar impedance  $I(\mathbf{x})$   
331 by the length of the elementary displacement:  $C(\mathbf{x}, \mathbf{x} + \delta\mathbf{x}) = I(\mathbf{x})\|\delta\mathbf{x}\|$ .

332 Hence, every displacement of length  $\|\delta\mathbf{x}\|$  around  $\mathbf{x}$  has the same cost what-  
 333 ever the direction ( $C$  is necessarily isotropic). This kind of formulation is easi-  
 334 ly solved in classical GIS softwares (it only requires to specify the impedance  
 335 raster, and the start and end points). However, we believe that our formula-  
 336 tion is preferable for steepest ascent/descent problems, which are anisotropic  
 337 in nature (see also Collischonn and Pilar, 2000).

338

339 Similarly, we can define a *downslope* cost function:

$$C_{\downarrow}(\mathbf{x}, \mathbf{x} + \delta\mathbf{x}) = \underbrace{+(\nabla z) \cdot \delta\mathbf{x}}_{(1)} - \underbrace{(-\|\nabla z\|\|\delta\mathbf{x}\|)}_{(2)} + \underbrace{\lambda\|\delta\mathbf{x}\|}_{(3)}$$

340 This time, (2) is the *minimum* elevation we could reach with a displace-  
 341 ment of length  $\|\delta\mathbf{x}\|$ . The difference (1) – (2) is always positive and is a  
 342 measure of *how much lower* we could have gotten with a displacement of  
 343 the same length: (1) and (2) cancel out in the case of a steepest *descent*.  
 344 Conversely, if we move upslope, (1) – (2) is large and the cost is high.

345

346 Finally, these cost functions satisfy the requirement that the steepest  
 347 ascent path from  $\mathbf{x}$  to  $\mathbf{x}'$  is also the steepest descent path from  $\mathbf{x}'$  to  $\mathbf{x}$   
 348 (assuming the same friction factor  $\lambda$ ):

$$C_{\uparrow}(\mathbf{x}, \mathbf{x}') = C_{\downarrow}(\mathbf{x}', \mathbf{x})$$

349 In the following, we only use the upslope cost function  $C_{\uparrow}$ ; we will see  
 350 why it is more convenient to treat the problem from downslope up. Moreover,  
 351 in order to improve flow convergence near the glacier boundary, we slightly  
 352 modify the cost function by increasing the friction factor  $\lambda$  near the boundary  
 353 (this will penalize flowlines wandering along the boundary):

$$C_{\uparrow}(\mathbf{x}, \mathbf{x} + \delta\mathbf{x}) = \|\nabla z\|\|\delta\mathbf{x}\| - (\nabla z) \cdot \delta\mathbf{x} + \underbrace{\left( \lambda_{\infty} + (\lambda_0 - \lambda_{\infty})e^{-\frac{D(\mathbf{x})}{D_{\lambda}}} \right)}_{\lambda(\mathbf{x})} \|\delta\mathbf{x}\|$$

354 where  $D(\mathbf{x})$  is the distance to the boundary at point  $\mathbf{x}$ ,  $\lambda_{\infty}$  is the friction  
 355 cost far from the boundary,  $\lambda_0 > \lambda_{\infty}$  is the friction cost at the boundary and  
 356  $D_{\lambda}$  is the scale of decrease with distance. Note that this modified cost is still

357 anisotropic:  $\lambda(\mathbf{x})$  is an impedance, but it is not the dominant term of the  
 358 cost function. The values  $\lambda_\infty = 0.035 \text{ m} \cdot \text{m}^{-1}$ ,  $\lambda_0 = 5\lambda_\infty = 0.175 \text{ m} \cdot \text{m}^{-1}$ ,  
 359 and  $D_\lambda = 150 \text{ m}$  were found to give very good results on all glaciers.

360

361 Finally, since we use a raster DEM (i.e. a square lattice with only 8  
 362 possible elementary displacements from a given grid point  $\mathbf{x}_{i,j}$ ), we define a  
 363 discrete version of  $C_\uparrow$ :

$$C_\uparrow(\mathbf{x}_{i,j}, \mathbf{x}_{i+\delta i, j+\delta j}) = \left( z_{i,j} + s_{\max} \sqrt{\delta i^2 + \delta j^2} \right) - z_{i+\delta i, j+\delta j} + \lambda(\mathbf{x}_{i,j}) \sqrt{\delta i^2 + \delta j^2}$$

364 where

$$s_{\max} = \max_{0 < (\delta i^2 + \delta j^2) \leq 2} \left\{ \frac{z_{i+\delta i, j+\delta j} - z_{i,j}}{\sqrt{\delta i^2 + \delta j^2}} \right\}$$

365 is the estimated upward slope (norm of the gradient) at pixel  $\mathbf{x}_{i,j}$ . If the  
 366 above expression for  $s_{\max}$  is negative, it is of course set to zero: there is a  
 367 local maximum at  $\mathbf{x}_{i,j}$ .

### 368 5.3. Cost assignment for paths between waypoints

369 We use Dijkstra's algorithm (Dijkstra, 1959) to compute the least-cost  
 370 path between each pair of waypoints. It uses the elementary cost function  
 371 to produce an accumulated cost surface spreading around a start point  $\mathbf{S}$ ,  
 372 and a backlink grid which gives the direction *opposite* to the gradient of the  
 373 accumulated cost surface at each pixel. The least-cost path from  $\mathbf{S}$  to any  
 374 point is constructed in the reverse direction, starting from the destination and  
 375 following the backlinks to  $\mathbf{S}$ . In our case, the cost is defined from downslope  
 376 up, so a backlink is defined from upslope down (see Figure 11).

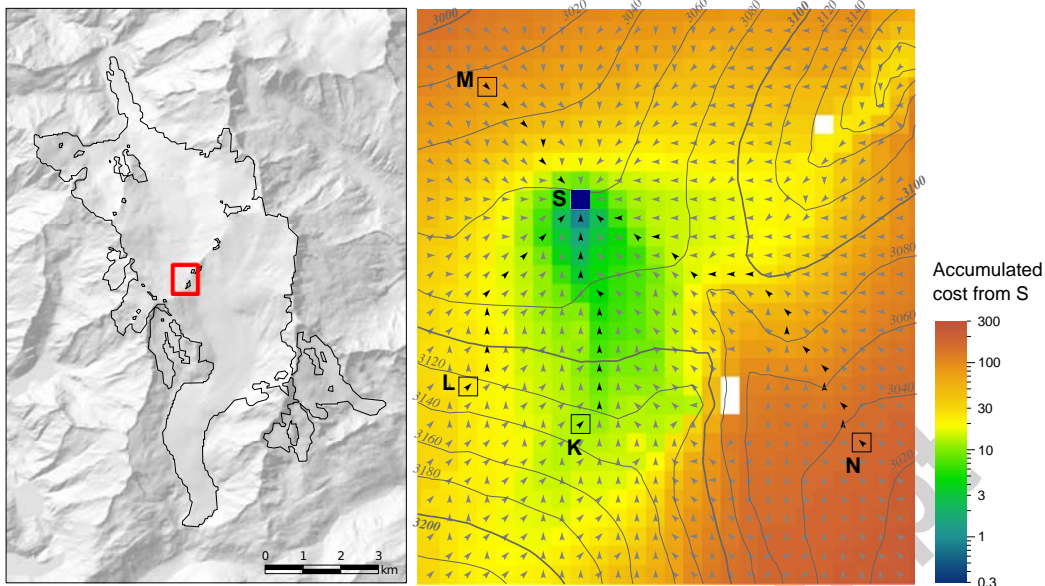


Figure 11: Example of accumulated cost surface, spreading from a start point **S**. Arrows indicate the backlinks: the least-cost path from **S** to any destination (**K**, **L**, **M**, **N**, etc.) is constructed from the destination to the start **S**, following the backlink grid. White pixels are ice-free zones (inner rocks) across which no displacement is possible.

377 Figure 11 illustrates the effects of the definition of  $C_{\uparrow}$ :

- 378
- 379 • destination **K** is located right upslope from start **S**, at an elevation of  
380 about 3130 m. Since edge (**S**,**K**) is almost a steepest ascent path, its  
381 cost is low:  $C_{\uparrow}(\mathbf{S}, \mathbf{K}) = 11.2$
  - 382 • destination **L** is located at about the same elevation, but one has to  
383 cross elevation contours at some angle to get there from **S**. The cost is  
384 higher:  $C_{\uparrow}(\mathbf{S}, \mathbf{L}) = 25.3$
  - 385 • destination **M** is located at an elevation lower than **S**, about 3030 m.  
386 Consequently, the edge from **S** to **M** is far from a steepest *ascent* (it is  
387 almost a steepest *descent*), and has a high cost:  $C_{\uparrow}(\mathbf{S}, \mathbf{M}) = 80.5$  (note  
388 that this path would in contrary have a very low cost with respect to  
the downslope cost function  $C_{\downarrow}$ )
  - 389 • finally, destination **N** is located on the other side of a ridge. In order  
390 to reach **N** from **S**, one must first climb to a pass at about 3100 m (low  
391 cost), but then go down (high cost). We have  $C_{\uparrow}(\mathbf{S}, \mathbf{N}) = 169.3$

392 We use this algorithm to compute the costs between any pair of skeletal  
 393 vertices/waypoints. In practice, we only compute the costs to the  $n$  nearest  
 394 neighbors of each vertex with respect to the cost function, using a local run  
 395 of Dijkstra’s algorithm that is aborted as soon as  $n$  neighbor vertices have  
 396 been visited (straightforward with an implementation based on a priority  
 397 queue). The value  $n = 30$  turned out to be largely sufficient for the following  
 398 steps. We obtain the kind of graph shown in Figure 12. Each edge can be  
 399 traversed in both directions, but at a different cost in each direction: the  
 400 graph is *directed*.

#### 401 5.4. Identification of minimum spanning branchings

402 The creation of a dense, redundant graph between the skeletal waypoints  
 403 looks like a step backwards, compared to the simplicity of the skeleton. How-  
 404 ever, graph theory provides powerful tools which will help simplify this graph  
 405 again, in the way we want.

406  
 407 Each waypoint (vertex) has several incoming and outgoing edges in the  
 408 new directed graph. The set of flowlines we are looking for is a *branching* or,  
 409 synonymously, a *directed spanning tree* i.e. a graph  $\mathcal{T}$  such that:

- 410 •  $\mathcal{T}$  contains no cycle,
- 411 • each vertex has *one and only one* incoming edge: each vertex is visited  
 412 (the tree is *spanning*), but no two edges of  $\mathcal{T}$  enter the same vertex  
 413 (i.e., each vertex has only one downstream pixel, since we build the  
 414 flowlines from downstream towards upstream).

415 Of course, such a tree  $\mathcal{T}$  has to be rooted at a snout, i.e. a special vertex  
 416 without an incoming edge. Moreover, we want the edges of this tree to be  
 417 —as much as possible— steepest climb routes, i.e. to have low costs with re-  
 418 spect to our cost function. Extracting a subset of edges (a subgraph) which  
 419 satisfies all these requirements (being a tree, being spanning, and having  
 420 a minimal cost) is a classical problem called Directed Minimum Spanning  
 421 Tree (DMST) extraction. It is efficiently solved with the Chu-Liu/Edmonds  
 422 algorithm (Chu and Liu, 1965; Edmonds, 1967): in this study we use the  
 423 implementation of Tofigh (2009), based on the Boost Graph Library (Siek et  
 424 al., 2002).

425



426 Since there are several snouts in a glacier complex, the subgraph may  
427 actually be a *forest* i.e. a set of trees, each one rooted at a different snout.  
428 The single-root version of the Edmonds algorithm is easily extended to the  
429 multiple-root case: a virtual ‘master’ root is created, and zero-cost edges are  
430 added from this root to each snout (see Figure 12).

431

432 Figure 13 shows the output of the algorithm for the Rhone-Trift glacier  
433 complex. It is worth noting that the segmentation of the complex into in-  
434 dividual glaciers is a by-product of the method: each snout ‘drains’ a set of  
435 upstream vertices which form its catchment.

436

Accepted manuscript

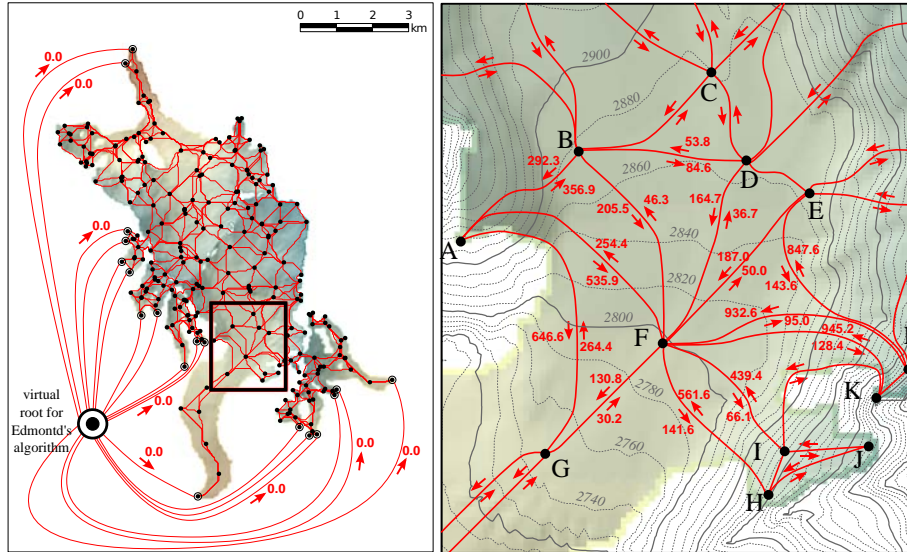


Figure 12: Edges and associated costs between skeleton waypoints in the Rhone-Trift glacier complex. Left: example of initial graph with numerous edges linking pairs of waypoints. For clarity, the plot displays only the edges between natural (planar) neighbors but a much denser graph can be created. Right: zoom on a region. Figures in red are the costs of each edge, in both directions.

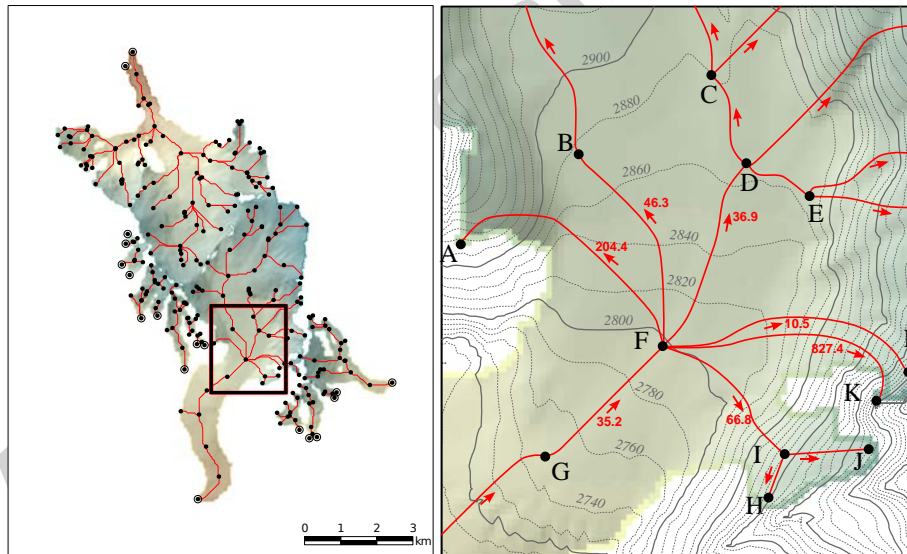


Figure 13: Output of the Chu-Liu/Edmonds algorithm with the set of edges and costs of Figure 12. The minimum branching (Directed Minimum Spanning Tree/Forest) allows to visit all waypoints, starting from a snout and always moving as upslope as possible.

437 Figure 14 is a zoom on a pass across the topographical divide between  
 438 Rhone and Trift glaciers (Undri Triftlimi). It explains why no edge in the  
 439 DMST/DMSF should cross any major topographical ridge. Let us suppose  
 440 that the ridge-crossing edge  $(\mathbf{K},\mathbf{L})$  is part of the DMSF, denoted  $\mathcal{F}$  and of  
 441 total cost  $C_{\uparrow}(\mathcal{F})$ . In this case, point  $\mathbf{L}$  ultimately drains to Trift glacier's  
 442 snout. However, the other incoming edge to  $\mathbf{L}$ ,  $(\mathbf{M},\mathbf{L})$ , has a lower cost than  
 443  $(\mathbf{K},\mathbf{L})$ : hence if we remove  $(\mathbf{K},\mathbf{L})$  from  $\mathcal{F}$  and add  $(\mathbf{M},\mathbf{L})$ , we obtain a forest  
 444  $\mathcal{F}'$  that is still spanning ( $\mathbf{L}$  is visited i.e. has an incoming edge) and has  
 445 a lower total cost  $C_{\uparrow}(\mathcal{F}') = C_{\uparrow}(\mathcal{F}) + C_{\uparrow}(\mathbf{M},\mathbf{L}) - C_{\uparrow}(\mathbf{K},\mathbf{L}) < C_{\uparrow}(\mathcal{F})$ . This  
 446 means that  $\mathcal{F}$  was not a DMSF in the first place (it is spanning but not of  
 447 minimum cost): point  $\mathbf{L}$  has to flow to Rhone glacier's snout, and no edge  
 448 should go through the pass. Hence, our procedure is efficient not only for  
 449 flowline extraction, but also for glacier segmentation.

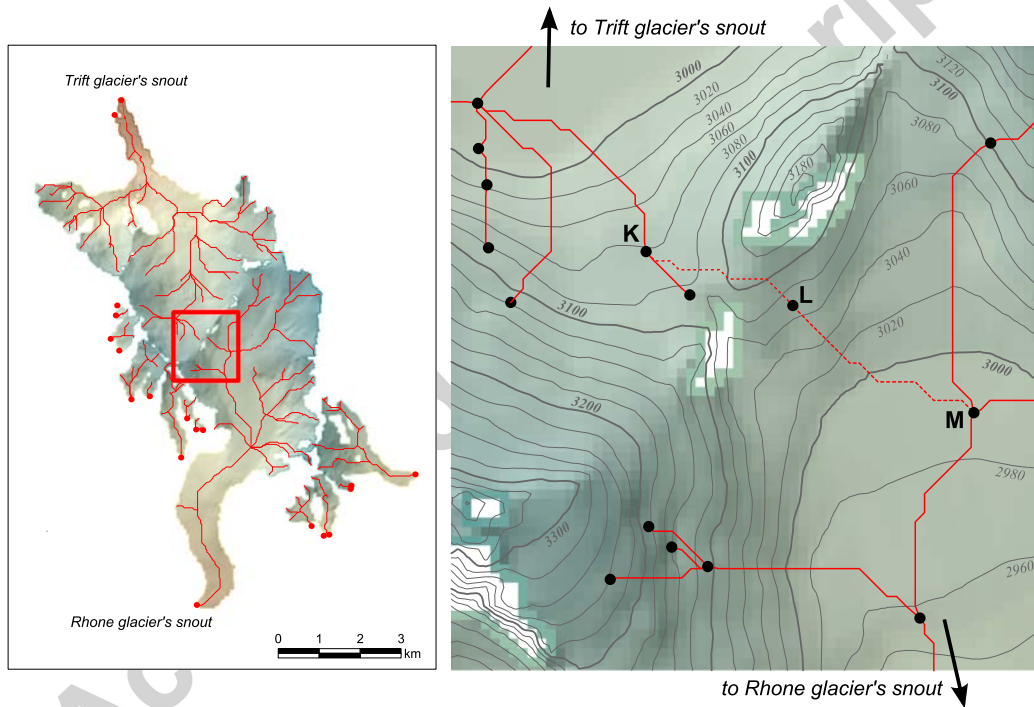


Figure 14: Zoom on the minimum branching in the vicinity of Undri Triftlimi, a pass on the divide between Rhone and Trift glaciers. Vertex  $\mathbf{L}$ , which is located south of the ridge, has to be visited from  $\mathbf{M}$  and not from  $\mathbf{K}$  in the Directed Minimum Spanning Tree/Forest: no edge should go across any major divide.

## 450 6. Conclusion and perspectives

451 In this paper we proposed a new method to extract glacier flowlines, based  
 452 on Voronoi skeletonization of glacier boundaries, skeleton pruning using Dis-  
 453 crete Curve Evolution (DCE), and the construction of a Directed Minimum  
 454 Spanning Tree between skeletal vertices with respect to an anisotropic, ups-  
 455 lope cost function  $C_{\uparrow}$ .

456  
 457 The application of the method requires limited parameter tweaking: it  
 458 only requires a selection rule  $k = f(A)$  for the level  $k$  of the DCE as a function  
 459 of glacier area  $A$  (2 parameters), and 3 parameters for the friction law (i.e.  
 460 the isotropic term of the cost function). Table 2 sums up the values used on  
 461 the whole domain of Figure 2a (1200 km<sup>2</sup> of glaciers, the largest contiguous  
 462 icefield having an area of 261 km<sup>2</sup>).

DCE level selection $k = 2 + \lfloor k_0 A^\gamma \rfloor$	$k_0$	13.5
	$\gamma$	0.8
Cost function $C_{\uparrow}(\mathbf{x}, \mathbf{x} + \delta\mathbf{x}) = \ \nabla z\  \ \delta\mathbf{x}\  - (\nabla z) \cdot \delta\mathbf{x} + \lambda(\mathbf{x}) \ \delta\mathbf{x}\ $ with $\lambda(\mathbf{x}) = \lambda_\infty + (\lambda_0 - \lambda_\infty) e^{-\frac{D(\mathbf{x})}{D_\lambda}}$	$\lambda_\infty$	0.035 m · m <sup>-1</sup>
	$\lambda_0$	0.175 m · m <sup>-1</sup>
	$D_\lambda$	150 m

Table 2: Parameters of the method.

463 The method currently lacks a quality assessment, though this could be  
 464 done on a small subset of glaciers by comparison with manually-extracted  
 465 flowlines. The large-scale visual assessment is however very satisfying, and  
 466 the resulting network can be used to compute indices such as Strahler orders,  
 467 bifurcation ratios, etc. Many scaling properties of glaciers, such as volume-  
 468 are scaling (Bahr et al., 1997) or power-law behavior of accumulation basin  
 469 areas (Gsell et al., 2014), originate in glacier branching topology: such prop-  
 470 erties could act as a ‘lever arm’ for tackling the problem of catchment-scale  
 471 glacier flow dynamics, much like other fundamental symmetries (plane-strain  
 472 or radial), as advocated by Bahr and Peckham (1996). We hope that this  
 473 study will foster ideas in this field.

## 474 7. Acknowledgments

475 This work has been supported by an EC2CO grant from the French CNRS  
 476 (INSU). The authors acknowledge the Swiss Federal Office of Topography  
 477 (SwissTopo) for providing the 25-meter DEM.

478 **8. References**

- 479 [1] Arendt, A., Bolch, T., Cogley, J. G., Gardner, A., Hagen, J. O., Hock,  
480 R., Kaser, G., et al., 2012. Randolph Glacier Inventory – A Dataset of  
481 Global Glacier Outlines: Version 3.2. Global Land Ice Measurements  
482 from Space, Boulder, CO, USA. Digital Media.  
483 URL <http://www.glims.org/RGI/>
- 484 [2] Bahr, D. B., Meier, M., Peckham, S. D., 1997. The physical basis of  
485 glacier volume-area scaling. *J. Geophys. Res.* 102, 20355–20362.
- 486 [3] Bahr, D. B., Peckham, S. D., 1996. Observations and analysis of self-  
487 similar branching topology in glacier networks. *J. Geophys. Res.* 101,  
488 25511–25521.
- 489 [4] Bai, X., Latecki, L. J., Liu, W.-Y., 2007. Skeleton pruning by contour  
490 partitioning with discrete curve evolution. *IEEE Trans. Pattern Anal.*  
491 *Mach. Intell.* 29 (3), 449–462.
- 492 [5] Barber, C. B., Dobkin, D. P., Huhdanpaa, H. T., 1996. The Quickhull al-  
493 gorithm for convex hulls. *ACM Trans. on Mathematical Software* 22 (2),  
494 469–483.  
495 URL <http://www.qhull.org>
- 496 [6] Blum, H., 1967. A Transformation for Extracting New Descriptors of  
497 Shape. In: Wathen-Dunn, W. (Ed.), *Models for the Perception of Speech*  
498 *and Visual Form*. MIT Press, Cambridge, pp. 362–380.
- 499 [7] Brandt, J. W., Algazi, V. R., 1992. Continuous skeleton computation  
500 by Voronoi diagram. *CVGIP: Image Understanding* 55 (3), 329–338.
- 501 [8] Chu, Y. J., Liu, T. H., 1965. On the shortest arborescence of a directed  
502 graph. *Science Sinica* 14, 1396–1400.
- 503 [9] Collischonn, W., Pilar, J. V., 2000. A direction dependent least-cost-  
504 path algorithm for roads and canals. *International Journal of Geographi-*  
505 *cal Information Science* 14 (4), 397–406.
- 506 [10] Dijkstra, E. W., 1959. A note on two problems in connexion with graphs.  
507 *Numerische Mathematik* 1, 269–271.  
508 URL <http://dx.doi.org/10.1007/BF01386390>

- 509 [11] Douglas, D. H., 1994. Least-cost Path in GIS Using an Accumulated  
510 Cost Surface and Slopelines. *Cartographica* 31 (3), 37–51.
- 511 [12] Edmonds, J., 1967. Optimum branchings. *J. Res. Natl. Bur. Stand.* 71B,  
512 233–240.
- 513 [13] Garbrecht, J., Martz, L. W., 1997. The assignment of drainage direction  
514 over flat surfaces in raster digital elevation models. *Journal of Hydrology*  
515 193 (1-4), 204–213.
- 516 [14] Gsell, P.-S., Le Moine, N., Moussa, R., Ribstein, P., 2014. Identifying  
517 the probabilistic structure of drained areas as a function of hypsometry  
518 in river networks. *Hydrological Processes*.  
519 URL <http://dx.doi.org/10.1002/hyp.10296>
- 520 [15] Gupta, V. K., Waymire, E., Wang, C. T., 1980. A representation of an  
521 instantaneous unit hydrograph from geomorphology. *Wat. Resour. Res.*  
522 16 (5), 855–862.
- 523 [16] Kienholz, C., Rich, J. L., Arendt, A. A., Hock, R., 2014. A new method  
524 for deriving glacier centerlines applied to glaciers in Alaska and north-  
525 west Canada. *The Cryosphere* 8 (2), 503–519.
- 526 [17] Latecki, L. J., Lakämper, R., 2002. Application of Planar Shape Com-  
527 parison to Object Retrieval in Image Databases. *Pattern Recognition*  
528 35, 15–29.
- 529 [18] Le Bris, R., Paul, F., 2013. An automatic method to create flow lines  
530 for determination of glacier length: A pilot study with Alaskan glaciers.  
531 *Computers & Geosciences* 52, 234–245.
- 532 [19] Le Moine, N., 2013. CLaRiNet: Catchment, Landform, and River Net-  
533 work analysis – A geomorphological toolbox for Scilab, User Manual  
534 (draft version). UPMC.  
535 URL <http://www.sisyphe.upmc.fr/~lemoine/resources.htm>
- 536 [20] Machguth, H., Huss, M., 2014. The length of the world’s glaciers – a  
537 new approach for the global calculations of center lines. *The Cryosphere*  
538 8, 1741–1755.

- 539 [21] Martz, L. W., Garbrecht, J., 1998. The treatment of flat areas and  
540 depressions in automated drainage analysis of raster digital elevation  
541 models. *Hydrological Processes* 12 (6), 843–855.
- 542 [22] Rodríguez-Iturbe, I., Valdés, J. B., 1979. The geomorphological struc-  
543 ture of the hydrologic response. *Wat. Resour. Res.* 15, 1409–1420.
- 544 [23] Scilab Enterprises, 2012. Scilab: Free and Open Source software for  
545 numerical computation. Scilab Enterprises, Orsay, France.  
546 URL <http://www.scilab.org>
- 547 [24] Siek, J. G., Lee, L.-Q., Lumsdaine, A., 2002. The Boost Graph Li-  
548 brary: User Guide and Reference Manual. Addison-Wesley, Boston,  
549 Massachusetts.  
550 URL <http://www.boost.org/doc/libs/release/libs/graph/>
- 551 [25] SwissTopo, 2004. DHM25, The digital height model of Switzerland,  
552 Product Information. Federal Office of Topography, Wabern, CH.
- 553 [26] Tofigh, A., 2009. Optimum Branchings and Spanning Arborescences.  
554 Accessed on SourceForge.  
555 URL <http://sourceforge.net/projects/edmonds-alg/>
- 556 [27] Warntz, W., 1957. Transportation, social physics, and the law of refraction.  
557 *The Professional Geographer* 9 (4), 2–7.  
558 URL [http://dx.doi.org/10.1111/j.0033-0124.1957.094\\_2.x](http://dx.doi.org/10.1111/j.0033-0124.1957.094_2.x)